
SEMI-SUPERVISED MACHINE LEARNING MODEL FOR LAGRANGIAN FLOW STATE ESTIMATION

A PREPRINT

Reno Miura

Department of Mechanical Engineering
Keio University
Yokohama 223-8522, Japan
renomiura0202@keio.jp

Koji Fukagata

Department of Mechanical Engineering
Keio University
Yokohama 223-8522, Japan
fukagata@mech.keio.ac.jp

November 16, 2023

ABSTRACT

In recent years, many researchers have demonstrated the strength of supervised machine learning for flow state estimation. Most of the studies assume that the sensors are fixed and the high-resolution ground truth can be prepared. However, the sensors are not always fixed and may be floating in practical situations — for example, in oceanography and river hydraulics, sensors are generally floating. In addition, floating sensors make it more difficult to collect the high-resolution ground truth. We here propose a machine learning model for state estimation from such floating sensors without requiring high-resolution ground-truth data for training. This model estimates velocity fields only from floating sensor measurements and is trained with a loss function using only sensor locations. We call this loss function as a "semi-supervised" loss function, since the sensor measurements are utilized as the ground truth but high-resolution data of the entire velocity fields are not required. To demonstrate the performance of the proposed model, we consider Stokes' second problem and two-dimensional decaying homogeneous isotropic turbulence. Our results reveal that the proposed semi-supervised model can estimate velocity fields with reasonable accuracy when the appropriate number of sensors are spatially distributed to some extent in the domain. We also discuss the dependence of the estimation accuracy on the number and distribution of sensors.

Keywords Fluid mechanics · Machine learning · State estimation · Floating sensors

1 Introduction

In the field of fluid mechanics and fluids engineering, state estimation from limited sensor measurements is an important task for applications to data assimilation, analysis of flow physics, and flow control. However, it is known that flow state estimation is very difficult because of the strong nonlinearities and the high degrees of freedom in space and time. As a method to deal with these issues, machine learning (ML) has recently been attracting attentions in flow estimation from limited sensor information (Kutz, 2017; Brenner *et al.*, 2019; Brunton *et al.*, 2020). ML is good at handling huge amounts of data containing a high degree of freedom and nonlinear dynamics of fluid flow phenomena (Brunton *et al.*, 2020). Many studies (Güemes *et al.*, 2019; Nair and Goza, 2020; Güemes *et al.*, 2021; Kumar *et al.*, 2022) have shown the superiority of ML over conventional state estimation methods such as proper orthogonal decomposition (POD)-based methods (Everson and Sirovich, 1995) and linear stochastic estimation (LSE) (Adrian and Moin, 1988). For instance, Erichson *et al.* (2020) proposed shallow neural networks (SNNs) for flow estimation from limited sensor measurements. The proposed SNNs was demonstrated by estimating a circular cylinder wake, sea surface temperature, and decaying homogeneous isotropic turbulence. They showed that the SNNs can accurately estimate the flow fields and outperforms the conventional method, *i.e.*, a POD-based method. In comparison between LSE and ML, Guasotni *et al.* (2020) utilized a convolutional neural network (CNN) (LeCun *et al.*, 1998) to estimate the velocity fields in a turbulent open channel flow, and demonstrated that ML is superior to LSE in terms of estimation accuracy. In addition,

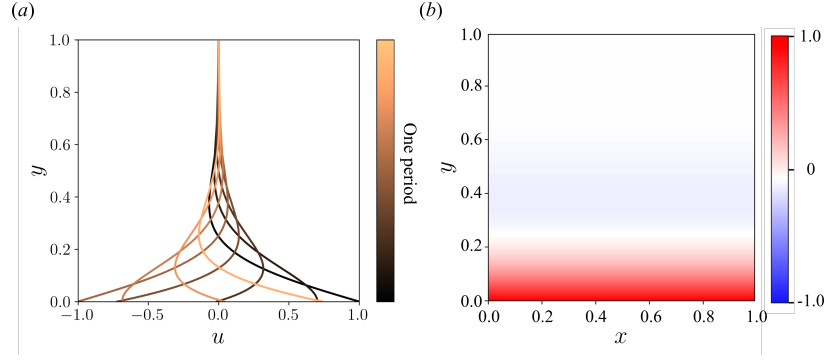


Figure 1: The calculated velocity u . (a) Time variation of the velocity profile in one period. (b) Velocity field at a certain time.

Nakamura *et al.* (2022) reported that ML can acquire higher noise robustness than LSE under appropriate problem settings and the amount of training data.

Most of those studies deal with situations in which the sensors are spatially fixed. Furthermore, they assume that reliable high-resolution ground truth can be prepared. Considering practical situations, however, the sensors are not always fixed and may be floating. For example, in oceanography (Wunsch and Heimbach, 2007; Laurindo *et al.*, 2017; Yu *et al.*, 2019) and river hydraulics (Tossavainen *et al.*, 2008; Tinka *et al.*, 2012; Landon *et al.*, 2014), sensors are generally not fixed and floating. Fukami *et al.* (2021) proposed a model that combines the Voronoi tessellation and CNN, and showed that can estimate the global flow field from sparse sensors that can be in motion and can change in numbers. However, there still remains the issue that ML-based models cannot be established without reliable high-resolution ground truth. In addition, floating sensors make it more difficult to collect reliable high-resolution ground truth than fixed sensors. Therefore, it should be attractive if one can construct an ML-based state estimator that can be trained without high-resolution ground truth.

In this study, we propose a machine-learning model to estimate velocity fields from floating sensors without requiring high-resolution data for training. This model estimates velocity fields only from floating sensor measurements and is trained with a loss function using only sensor measurements and locations. Specifically, only sensor location is utilized as the ground truth to define the loss function. We call this loss function as a "semi-supervised" loss function, since sensor measurements are used but high-resolution data of the entire velocity fields are not required. We evaluate the performance of the proposed method with simple problems, *i.e.*, Stokes' second problem and two-dimensional decaying homogeneous isotropic turbulence, and we investigate the dependence of the model performance on the number and distribution of sensors. The present paper is organized as follows. The preparation of the flow datasets and the sensor tracking method used in this study are provided in section 2. Details of the machine learning model and the semi-supervised loss function are explained in section 3. Results and discussion of the machine learning-based flow estimation are presented in section 4. We finally draw conclusions in section 5.

2 Datasets

2.1 Stokes' second problem

To demonstrate the capability of the proposed semi-supervised model in a simple example, the Stokes' second problem is considered first. The Stokes' second problem is the flow induced by an oscillating flat plate and known as one of the most basic unsteady problems having the exact solutions of the Navier-Stokes equations. We assume that a flat plate located at $y = 0$ is oscillating with a velocity $U \cos \omega t$ in x -direction, where U is the oscillation amplitude and ω is the angular frequency of oscillation. As is well known, the Navier-Stokes equation in x -direction in this case reduces to

$$\frac{\partial u}{\partial t} = \nu \frac{\partial^2 u}{\partial y^2}, \quad (1)$$

where $u(y, t)$ is the velocity in x -direction, and ν is the kinematic viscosity. Under the boundary conditions,

$$u(0, t) = U \cos \omega t, \quad u(\infty, t) = 0, \quad (2)$$

the exact solution is obtained as (Landau and Lifshitz, 1987)

$$u(y, t) = U e^{-ky} \cos(ky - \omega t), \quad \text{where } k = \sqrt{\frac{\omega}{2\nu}}. \quad (3)$$

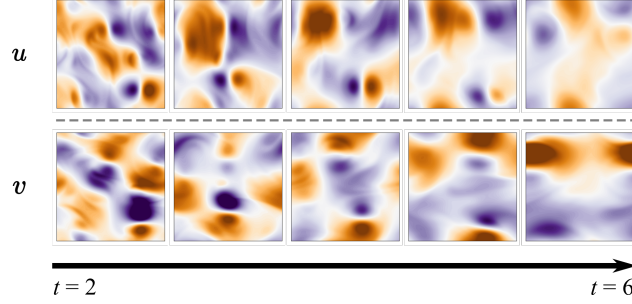


Figure 2: Velocity fields of two-dimensional decaying homogeneous isotropic turbulence at the initial Reynolds number $\text{Re}_0 = 177$.

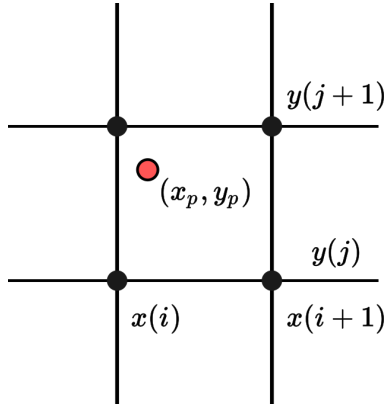


Figure 3: Relationship between a computational grid and a sensor location desired to be interpolated.

In this study, we consider the velocity field in which this exact solution is distributed over two-dimensional equally spaced grid points. The computational domain size is $(L_x, L_y) = (1, 1)$, and the number of the grid points is $(N_x, N_y) = (128, 128)$. The amplitude and frequency of the flat plate oscillation are set to $U = 1$ and $\omega = 4$, respectively, and the kinematic viscosity of $\nu = 0.05$ is assumed. For the present demonstration, we prepare 1000 snapshots with the time interval $\Delta t = \sqrt{2}/100$. The irrational (i.e. $\sqrt{2}$) time interval is adopted so that each snapshot gathered in a long period of time has different information. The profile and the field of the calculated velocity u is visualized in figure 1.

2.2 Two-dimensional decaying homogeneous isotropic turbulence

As the second example, we consider the two-dimensional decaying homogeneous isotropic turbulence. The training data set is prepared by a direct numerical simulation (DNS) (Taira *et al.*, 2016) solving the two-dimensional vorticity transport equation,

$$\frac{\partial \omega}{\partial t} + \mathbf{u} \cdot \nabla \omega = \frac{1}{\text{Re}_0} \nabla^2 \omega, \quad (4)$$

where $\mathbf{u} = (u, v)$ and ω are the velocity and vorticity, respectively. The size of the computational domain is $L_x = L_y = 1$. In this study, we consider the initial Reynolds number $\text{Re}_0 \equiv u_0^* l_0^* / \nu = 177$, where $u_0^* \equiv [\overline{u^2}(t_0)]^{1/2}$ is the characteristic velocity given by the square-root of the spatially averaged initial kinetic energy, $l_0^* = [2\overline{u^2}(t_0)/\overline{\omega^2}(t_0)]^{1/2}$ is the initial integral length, and ν is the kinematic viscosity. The number of grid points is $N_x = N_y = 256$. For the input sensor measurements and the required outputs to the semi-supervised model, the velocity $\mathbf{u} = (u, v)$ as shown in figure 2 is utilized. We use 1000 snapshots for the training of the present model. The time range is a dimensionless time of $2 \leq t \leq 6$ with a time interval of $\Delta t = 0.004$.

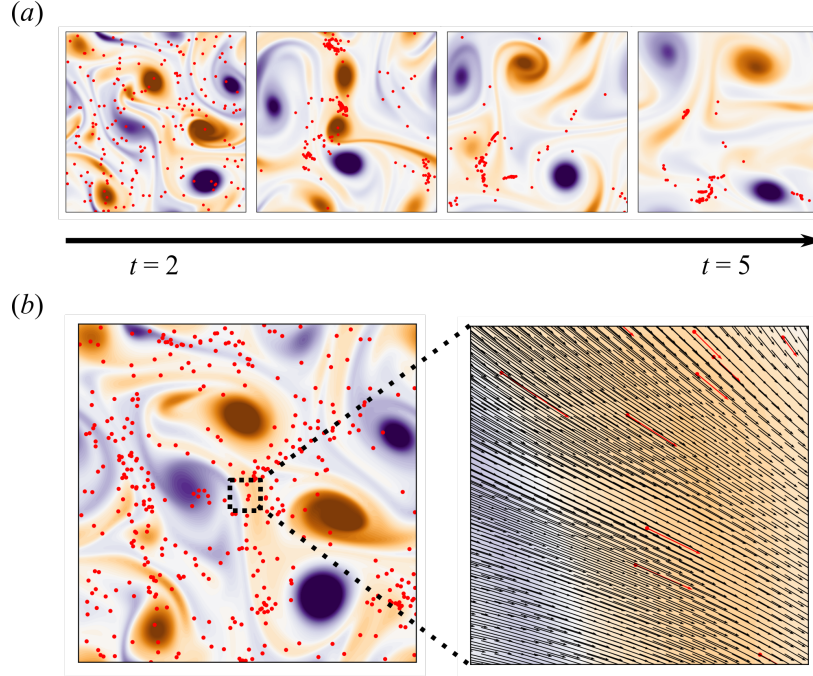


Figure 4: Sensors tracking in the two-dimensional decaying turbulence at initial Reynolds number $Re_0 = 177$. (a) Time variation of sensor distribution. (b) Relationship between the fluid velocity and the sensor velocity. The black vectors represent the fluid velocity, and the red vectors represent the sensor velocity.

2.3 Sensor tracking method

The behavior of floating sensors is computed by Lagrangian particle tracking. The datasets of the flow fields are computed using an Eulerian description, while the movement of the sensors is computed using a Lagrangian description focusing on each sensor. In this study, we assume that sensors are tracer particles that perfectly follow the flow field; namely, the velocity of the sensor \mathbf{u}_p is simply expressed as

$$\mathbf{u}_p = \mathbf{u}_f(\mathbf{x}_p), \quad (5)$$

where \mathbf{x}_p is the sensor location and \mathbf{u}_f is the fluid velocity. In order to obtain the fluid velocity at the sensor locations, the bilinear interpolation is used. Figure 3 shows the relationship between an orthogonal computational grid for the fluid velocity \mathbf{u}_f and a sensor position to be interpolated. Using bilinear interpolation, the fluid velocity at the sensor location \mathbf{x}_p is given by,

$$\mathbf{u}_f(\mathbf{x}_p) = (1 - \alpha)(1 - \beta)\mathbf{u}_{ij}^f + \alpha(1 - \beta)\mathbf{u}_{i+1j}^f + \alpha\beta\mathbf{u}_{i+1j+1}^f + (1 - \alpha)\beta\mathbf{u}_{i+1j}^f, \quad (6)$$

where the weighting factors α and β are $\alpha = (x_p - x(i))/\Delta x$ and $\beta = (y_p - y(j))/\Delta y$, respectively. The Crank-Nicholson method is used for the time integration method and the sensor position \mathbf{x}_p^{n+1} at the next time step $t = (n + 1)\Delta t$ is given by

$$\mathbf{x}_p^{n+1} = \mathbf{x}_p^n + \frac{\Delta t}{2}(\mathbf{u}_p^n + \mathbf{u}_p^{n+1}), \quad (7)$$

where the time integration interval should be the same as the flow datasets. In addition, sensor-to-sensor collisions are ignored.

Figure 4 (a) shows the time variation of the sensor distribution when 200 sensors are tracked in the two-dimensional decaying turbulence at the initial Reynolds number $Re_0 = 177$. As shown in figure 4 (a), most of the sensors are captured at a few locations over time in the two-dimensional decaying turbulence. In the previous study (Wilczek *et al.*, 2008), it was reported that in two-dimensional decaying turbulence, tracer particles are affected by the velocity field of a single eddy, so that the velocity of the particles decays as the eddy structure increases, and they remain at the same location for a long time. The present sensor tracking result is qualitatively consistent with the phenomenon shown by the previous study. In addition, since sensors are assumed to be tracer particles in this study, the velocity of the fluid

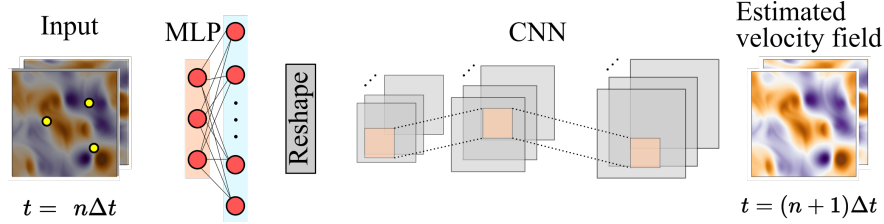


Figure 5: Schematic of MLP-CNN model for estimation of velocity fields at the next time step.

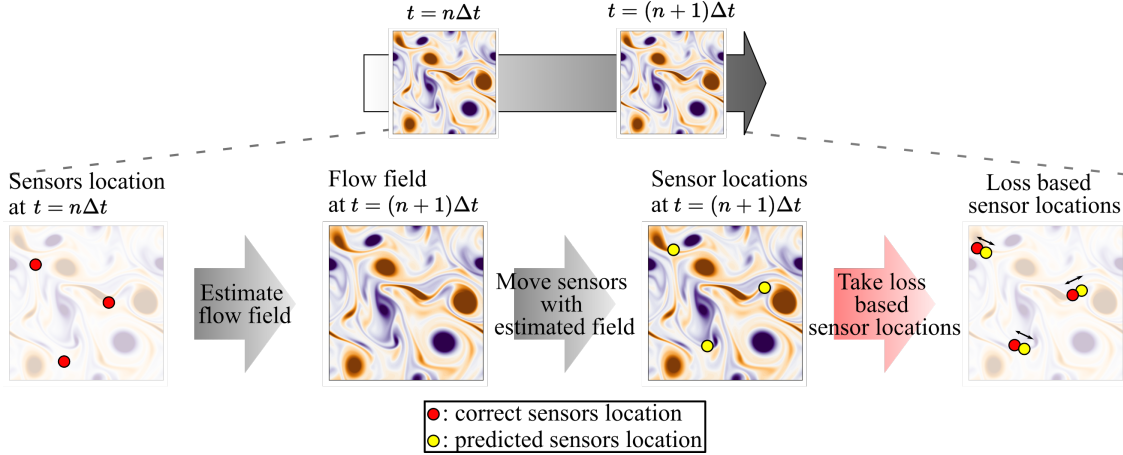


Figure 6: Schematic of the semi-supervised training process.

and the velocity of the sensors should be identical. The visualization of the vector of the fluid velocity and the sensor velocity is shown in figure 4 (b). The black vectors represent the fluid velocity vectors and the red vectors represent the sensor velocity vectors. As shown in figure 4 (b), the velocity of the sensors at any given position is in agreement with the velocity of the fluid.

3 Methods

3.1 Machine learning model

In this study, we utilize a network that combines a multi-layer perceptron (MLP) (Rumelhart *et al.*, 1986) and a convolutional neural network (CNN) (LeCun *et al.*, 1998). As shown in figure 5, the MLP-CNN model expands the dimension of input sensor measurements by MLP and CNN with upsampling layers, and outputs the entire velocity fields at the next time step. We attempt to train the MLP-CNN model through a semi-supervised loss function as will be explained in section 3.2.

3.2 Semi-supervised loss function

In this study, we aim to construct a machine learning model that does not require high-resolution flow field data, and train it using a loss function that utilizes sensor location information. Figure 6 shows the training process of a machine learning model. The training process is divided into three steps.

1. Estimation of entire velocity fields at the next time step from sensor measurements

First, the velocity sensor measurements and locations are used to estimate the entire velocity fields at the next time step. The MLP-CNN presented in section 3.1 is used as the machine learning model to estimate the entire velocity fields. That is, using the fluid velocity at the sensor position \mathbf{u}_f^n , the velocity field at the next time step \mathbf{u}^{n+1} is obtained as,

$$\tilde{\mathbf{u}}^{n+1} = \mathcal{F}(\mathbf{u}_f^n), \quad (8)$$

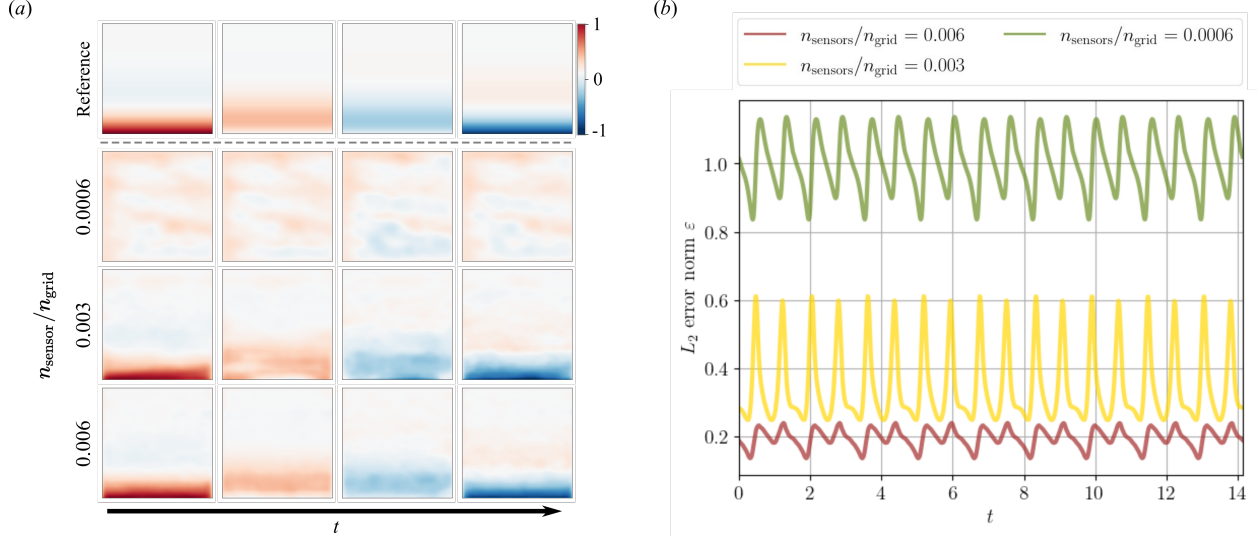


Figure 7: Dependence on the number of sensors in the case of Stokes' second problem. (a) Time variation of the estimated velocity field in one period. (b) Time variation of the L_2 error norm ϵ .

where $\tilde{(\cdot)}$ denotes the estimated value, and \mathcal{F} is a machine learning model that estimates the entire velocity fields from the sensor measurements. We aim to train the machine learning model \mathcal{F} without high-resolution flow field data.

2. Prediction of sensor locations using the estimated velocity fields

Next, the estimated entire velocity fields $\tilde{\mathbf{u}}^{n+1}$ are used to predict the sensor location at the next time step $\tilde{\mathbf{x}}_p^{n+1}$. The sensor location is predicted using the sensor tracking method explained in section 2.3. Thus, the sensor location at the next time step \mathbf{x}_p^{n+1} is obtained as,

$$\tilde{\mathbf{x}}_p^{n+1} = \mathcal{G}(\mathbf{x}_p^n, \mathbf{u}_f^n, \tilde{\mathbf{u}}_f^{n+1}), \quad (9)$$

where \mathcal{G} denotes the sensor tracking method and $\tilde{\mathbf{u}}_f^{n+1}$ is the velocity of the fluid at the sensor location obtained by interpolating the estimated entire velocity fields $\tilde{\mathbf{u}}^{n+1}$.

3. Loss function based on sensor location information

Finally, the loss function $\tilde{\mathbf{x}}_p^{n+1}$ defined with the predicted sensor locations $\tilde{\mathbf{x}}_p^{n+1}$ and the correct sensor locations \mathbf{x}_{ref} is computed to optimize the weights ω of the machine learning model \mathcal{F} . Therefore, the problem setting in this study results in an optimization problem, *i.e.*,

$$\omega = \operatorname{argmin}_{\omega} \|\mathbf{x}_{\text{ref}} - \mathcal{G}(\mathbf{x}_p^n, \mathbf{u}_f^n, \tilde{\mathbf{u}}_f^{n+1})\|_2. \quad (10)$$

As described above, the machine learning model developed in this study does not require high-resolution flow field data and can be trained using only sensor information. We call the loss function shown on the right-hand side of equation 10 as a "semi-supervised" loss function.

4 Results and discussion

4.1 Example 1: Stokes' second problem

As a demonstration for the one-dimensional flow field, we first estimate the entire velocity field calculated based on the exact solution of Stokes' second problem. We construct a semi-supervised learning-based MLP-CNN model that estimates the velocity field \mathbf{u} using the sensor velocity \mathbf{u}_p as input data. Here, we examine the dependence of estimation accuracy on the number of sensors. Specifically, three different ratios of the number of sensors to the total number of grid points $n_{\text{sensor}}/n_{\text{grid}} = \{0.0006, 0.003, 0.006\}$ (*i.e.*, 0.06%, 0.03% and 0.6% of the total number of grid points)

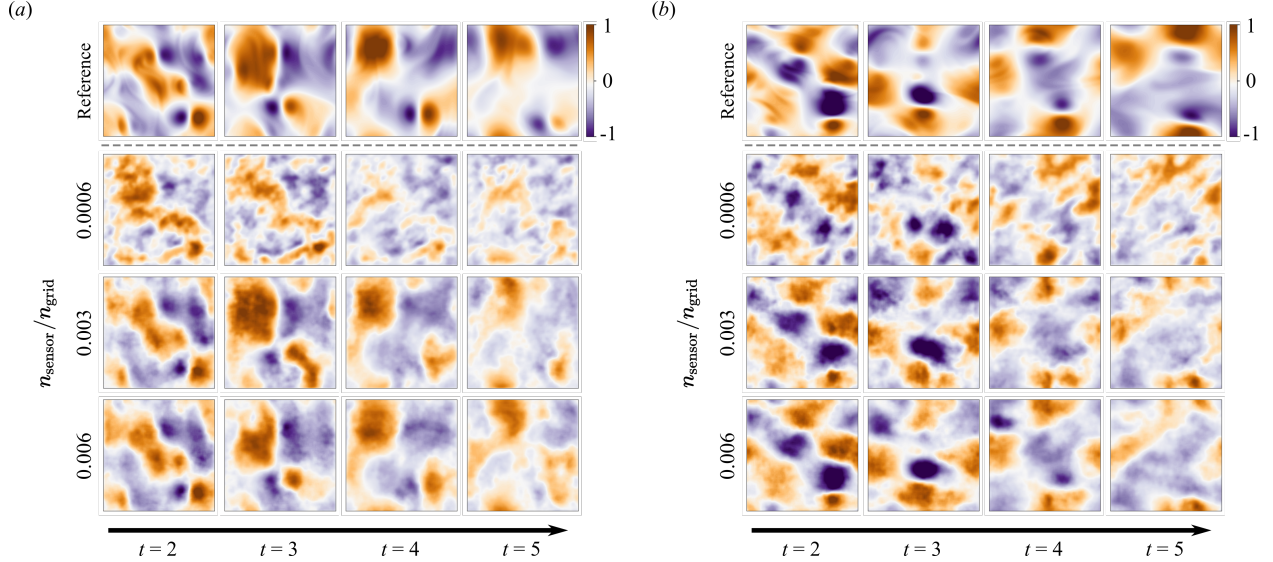


Figure 8: Dependence on the number of sensors in the case of two-dimensional decaying turbulence. Visualization of estimated velocity fields of (a) u component, (b) v component.

are considered. In this study, separate models are constructed and evaluated depending on the number of sensors, but the number of weights in each model is the same.

The velocity fields estimated from each number of sensors within a cycle are visualized in figure 7 (a). As shown, the flow structure can roughly be estimated for the ratios of $n_{\text{sensor}}/n_{\text{grid}} = \{0.003, 0.006\}$. The estimation becomes more difficult as the number of sensors is reduced, and we can confirm that the present model is highly dependent on the number of sensors. Figure 7 (b) shows the time variation of the L_2 error norm defined by $\epsilon = \|\mathbf{q}_{\text{DNS}} - \mathbf{q}_{\text{ML}}\|_2 / \|\mathbf{q}'_{\text{DNS}}\|_2$. In terms of the L_2 error norm, the present model also shows a high dependence of estimation accuracy on the number of sensors. It can also be seen that the L_2 error norm is periodically and sharply increasing or decreasing. The L_2 error norm reaches its maximum value at the time when a rapid velocity change occurs in the cycle of the flow field. The model is trained by estimating the velocity field at the next time from the velocity measurements at one time and then using both to predict the sensor location at the next time. Therefore, the model has difficulty dealing with abrupt changes in the flow field.

4.2 Example 2: Two-dimensional decaying turbulence

Next, as an example of a two-dimensional flow field, we estimate the velocity fields of the two-dimensional isotropic decaying turbulence. A semi-supervised learning-based MLP-CNN model is constructed to estimate the velocity fields \mathbf{u} using sensor velocity measurements \mathbf{u}_p as input data.

As in section 4.1, we evaluate the model in three cases where the ratio of the number of sensors to the total computed grid points is $n_{\text{sensor}}/n_{\text{grid}} = \{0.0006, 0.003, 0.006\}$ and investigate the dependency of the estimation accuracy on the number of sensors. The velocity fields estimated from each number of sensors are visualized in figure 8. When the ratio of the number of sensors to the total computed grid points is $n_{\text{sensor}}/n_{\text{grid}} = \{0.003, 0.006\}$, it can be seen that the flow structure is roughly captured although the details are not. The time variation of the L_2 error norm in each case of $n_{\text{sensor}}/n_{\text{grid}} = \{0.0006, 0.003, 0.006\}$ is shown in figure 9. As in the case of Stokes' second problem, the accuracy of the estimation decreases significantly as the number of sensors is reduced. This indicates that the present model is highly dependent on the number of sensors. In addition, it can be confirmed that the estimation accuracy decreases with time. This is due to the fact that in two-dimensional decaying turbulence, the sensor is trapped in a single vortex over time, as shown in section 2.3.

To investigate the effect of this sensor particle trapping, the particle number density is calculated with the weight function,

$$w_{ij} = \begin{cases} \frac{r_e}{|\mathbf{r}_{ij}|} & (0 \leq |\mathbf{r}_{ij}| \leq r_e) \\ 0 & (r_e < |\mathbf{r}_{ij}|) \end{cases}, \quad (11)$$

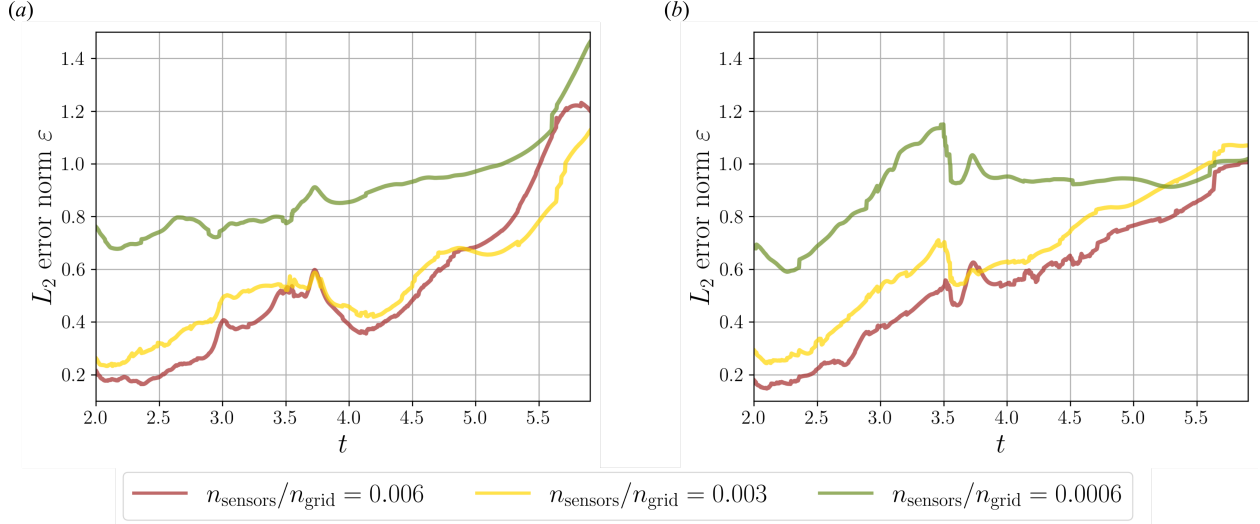


Figure 9: Dependence of the L_2 error norm on the number of sensors. Time variation of the L_2 error norm for (a) the u component and (b) the v component.

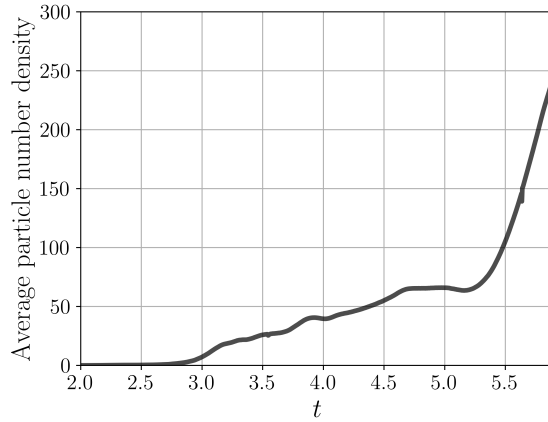


Figure 10: Time evolution of average particle number density in the case of $n_{\text{sensor}}/n_{\text{grid}} = 0.003$.

where r_{ij} is the distance between the i th particle and the j th particle, and r_e is a specific parameter, the radius of influence. With this weight function, the particle number density is obtained as

$$n_i = \sum_{j \neq i} w_{ij}. \quad (12)$$

In this study, the radius of influence is set to $r_e = 0.005$, and equation 12 is calculated for all sensors at each time step, and the mean particle number density at each time is calculated. Figure 10 shows the time evolution of the mean particle number density in the case of $n_{\text{sensor}}/n_{\text{grid}} = 0.003$. The overall trend is that the mean particle number density increases with time, corresponding to the decrease in estimation accuracy in figure 8. The mean particle number density generally increases with time, corresponding to the decrease in estimation accuracy in figure 8. This suggests that the estimation accuracy of the model is strongly influenced by the distribution of sensors over the region.

5 Conclusions

In this study, we constructed a semi-supervised learning-based machine learning model to estimate the entire velocity fields using only floating sensor measurements and location information, without requiring high-resolution fluid data as training data. We demonstrated the model with Stokes' second problem and the two-dimensional decaying

homogeneous isotropic turbulence as examples, and we investigated its dependence of estimation accuracy on the number and distribution of sensors. The model was able to estimate the rough structures of the velocity fields without high-resolution data, provided that the floating sensors are distributed in the appropriate number and location. Since the model does not utilize high-resolution flow field data, it is important to prepare an appropriate number and distribution of sensors. We expect that the present machine-learning-based estimator will be useful in the situations where we want to roughly estimate velocity fields when the high-resolution ground-truth flow field data are unavailable.

References

- Adrian, R. J. and Moin, P. (1988), “Stochastic estimation of organized turbulent structure: homogeneous shear flow”, *Journal of Fluid Mechanics*, Vol. 190, pp. 531–559.
- Brenner, M. P., Eldredge, J. D., and Freund, J. B. (2019), “Perspective on machine learning for advancing fluid mechanics”, *Physical Review Fluids*, Vol. 4 (10), 100501.
- Brunton, S. L., Hemati, M. S., and Taira, K. (2020), “Special issue on machine learning and data-driven methods in fluid dynamics”, *Theoretical and Computational Fluid Dynamics*, Vol. 34 (4), pp. 333–337.
- Brunton, S. L., Noack, B. R., and Koumoutsakos, P. (2020), “Machine learning for fluid mechanics”, *Annual review of fluid mechanics*, Vol. 52, pp. 477–508.
- Erichson, N. B., Mathelin, L., Yao, Z., Brunton, S. L., Mahoney, M. W., and Kutz, J. N. (2020), “Shallow neural networks for fluid flow reconstruction with limited sensors”, *Proceedings of the Royal Society A*, Vol. 476 (2238), 20200097.
- Everson, R. and Sirovich, L. (1995), “Karhunen–Loeve procedure for gappy data”, *JOSA A*, Vol. 12 (8), pp. 1657–1664.
- Fukami, K., Maulik, R., Ramachandra, N., Fukagata, K., and Taira, K. (2021), “Global field reconstruction from sparse sensors with Voronoi tessellation-assisted deep learning”, *Nature Machine Intelligence*, Vol. 3 (11), pp. 945–951.
- Guastoni, L., Encinar, M. P., Schlatter, P., Azizpour, H., and Vinuesa, R. (2020), “Prediction of wall-bounded turbulence from wall quantities using convolutional neural networks”, In *Journal of Physics: Conference Series*, (Vol. 1522, No. 1, p. 012022). IOP Publishing.
- Güemes, A., Discetti, S., and Ianiro, A. (2019), “Sensing the turbulent large-scale motions with their wall signature”, *Physics of Fluids*, Vol. 31 (12).
- Güemes, A., Discetti, S., Ianiro, A., Sirmacek, B., Azizpour, H., and Vinuesa, R. (2021), “From coarse wall measurements to turbulent velocity fields through deep learning”, *Physics of Fluids*, Vol. 33 (7).
- Kumar, Y., Bahl, P., and Chakraborty, S. (2022), “State estimation with limited sensors—a deep learning based approach”, *Journal of Computational Physics*, Vol. 457, 111081.
- Kutz, J. N. (2017), “Deep learning in fluid dynamics. Journal of Fluid Mechanics”, *Journal of Fluid Mechanics*, Vol. 814, pp. 1–4.
- Landon, K. C., Wilson, G. W., Özkan-Haller, H. T., and MacMahan, J. H. (2014), “Bathymetry estimation using drifter-based velocity measurements on the Kootenai River, Idaho”, *Journal of Atmospheric and Oceanic Technology*, Vol. 31 (2), pp. 503–514.
- Landau, L. D. and Lifshitz, E. M. (1987), “Fluid Mechanics, 2nd edition: Landau and Lifshitz: Course of Theoretical Physics, Volume 6”, Elsevier, pp. 83–85.
- Laurindo, L. C., Mariano, A. J., and Lumpkin, R. (2017), “An improved near-surface velocity climatology for the global ocean from drifter observations”, *Deep Sea Research Part I: Oceanographic Research Papers*, Vol. 124, pp. 73–92.
- LeCun, Y., Bottou, L., Bengio, Y., and Haffner, P. (1998), “Gradient-based learning applied to document recognition”, *Proceedings of the IEEE*, Vol. 86 (11), pp. 2278–2324.
- Nair, N. J. and Goza, A. (2020), “Leveraging reduced-order models for state estimation using deep learning”, *Journal of Fluid Mechanics*, Vol. 897, R1.
- Nakamura, T., Fukami, K., and Fukagata, K. (2022), “Identifying key differences between linear stochastic estimation and neural networks for fluid flow regressions”, *Scientific reports*, Vol. 12 (1), 3726.
- Rumelhart, D. E., Hinton, G. E., and Williams, R. J. (1986), “Learning representations by back-propagating errors”, *nature*, Vol. 323 (6088), pp. 533–536.
- Taira, K., Nair, A. G., and Brunton, S. L. (2016), “Network structure of two-dimensional decaying isotropic turbulence”, *Journal of Fluid Mechanics*, Vol. 795, R2.

- Tinka, A., Rafiee, M., and Bayen, A. M. (2012), “Floating sensor networks for river studies”, *IEEE Systems Journal*, Vol. 7 (1), pp. 36–49.
- Tossavainen, O. P., Percelay, J., Tinka, A., Wu, Q., and Bayen, A. M. (2008), “Ensemble kalman filter based state estimation in 2d shallow water equations using lagrangian sensing and state augmentation”, In *2008 47th IEEE Conference on Decision and Control*, (pp. 1783-1790). IEEE.
- Wilczek, M., Kamps, O., and Friedrich, R. (2008), “Lagrangian investigation of two-dimensional decaying turbulence”, *Physica D: Nonlinear Phenomena*, Vol. 237 (14-17), pp. 2090–2094.
- Wunsch, C., and Heimbach, P. (2007), “Practical global oceanic state estimation”, *Physica D: Nonlinear Phenomena*, Vol. 230 (1-2), pp. 197–208.
- Yu, X., Ponte, A. L., Elipot, S., Menemenlis, D., Zaron, E. D., and Abernathey, R. (2019), “Surface kinetic energy distributions in the global oceans from a high-resolution numerical model and surface drifter observations”, *Geophysical Research Letters*, Vol. 46 (16), pp. 9757–9766.